

An investigation on tunnel deformation behavior of expressway tunnels

Shong-Loong Chen* and Shen-Chung Lee^a

Department of Civil Engineering, National Taipei University of Technology, Taiwan (ROC)

(Received December 11, 2019, Revised February 16, 2020, Accepted March 2, 2020)

Abstract. The magnitude and distribution of tunnel deformation were widely discussed topics in tunnel engineering. In this paper, a three-dimensional (3D) finite element program was used for the analysis of various horseshoe-shaped opening expressway tunnels under different geologies. Two rock material models — Mohr-Coulomb and Hoek-Brown were executed in the process of analyses; and the results show that the magnitude and distribution of tunnel deformation were close by these two models. The tunnel deformation behaviors were relevant to many factors such as cross-sections and geological conditions; but the geology was the major factor to the normalized longitudinal deformation profile (LDP). If the time-dependent factors were neglected, the maximum displacements were located at the distance of 3 to 4 tunnel diameters behind the excavation face. The ratios of displacement at the excavation face to the maximum displacement were around 1/3 to 1/2. In general, the weaker the rock mass, the larger the ratio. The displacements in front of the excavation face were decreased with the increase of distance. At the distance of 1.0 to 1.5 tunnel diameter, the displacements were reduced to one-tenth of the maximum displacement.

Keywords: expressway tunnel; longitudinal deformation profile (LDP); excavation face; material model

1. Introduction

The evaluation of excavation deformation behaviors is essential for the design and construction of tunnels. Factors that have influence on tunnel deformation include, for example, the properties of rock mass, initial stresses, tunnel support and construction steps, all of which are related to the excavation of tunnel one way or the other. Considering the complexity of geology and the flexible application of tunneling method, the deformation of a tunnel and its distribution are very difficult to estimate, particularly the pre-deformation behaviors in front of the excavation face.

In general, the longitudinal deformation profile (LDP) is the distribution of radial displacement of a tunnel along the direction in which the tunnel is excavated. This profile covers the section in front of excavation face (excavated section) and the one behind (unexcavated section). The LDP has been investigated in several previous studies. Previous studies indicate that the deformation is created approximately 1.5 to 2.5 times of tunnel diameter in front of the excavation face, and reaches its maximum roughly 2 to 4 times of tunnel diameter behind the excavation face.

For the convenience of analysis, the cross section of tunnel in previous studies is mostly assumed to be circular. However, most of today's tunnels that are excavated by drill and blast method have a cross section in the shape of a horseshoe for the engineering economy and stability, and

the steps of tunnel excavation, round length and primary support vary widely depending on the properties of rock mass and the size of cross section. In this study, the tunnels along the expressways of Taiwan are selected as the examples due to the engineering practicality. Three different cross sections, one-lane, two-lane and three-lane, are investigated for the tunnel deformation behaviors at various geological conditions. The analysis result suggests that, while the tunnel deformation behaviors vary with geology and cross section, the geology is still the most significant factor that has influence on the LDP of a tunnel after normalization.

2. Literature review

Assuming that a circular tunnel is surrounded by a homogeneous, isotropic and continuous material, Brady and Brown determined the deformation in the rock mass surrounding the tunnel using the elasticity theory of planar strain lines, as shown in Eqs. (1) and (2).

$$u_r = -\frac{P_v R^2 (1 + \nu)}{2Er} \times \left\{ (1 + k) - (1 - k) \left[4(1 - \nu) - \frac{R^2}{r^2} \right] \cos 2\theta \right\} \quad (1)$$

$$u_\theta = -\frac{P_v R^2 (1 + \nu)}{2Er} \left\{ (1 - k) \left[2(1 - 2\nu) + \frac{R^2}{r^2} \right] \sin 2\theta \right\} \quad (2)$$

For Eqs. (1) and (2) above, u_r and u_θ are radial and

*Corresponding author, Ph.D., Professor

E-mail: f10391@ntut.edu.tw

^aPh.D.

E-mail: sclee.geo@msa.hinet.net

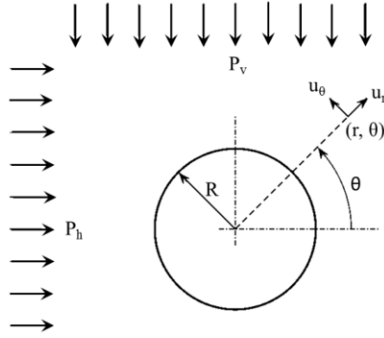


Fig. 1 Displacements around a circular tunnel located in a biaxial stress field (After Brady and Brown 1993).

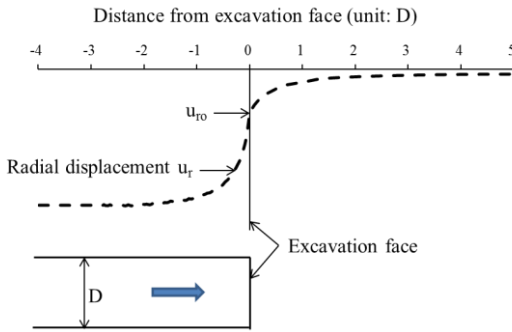


Fig. 2 Longitudinal deformation profile of a circular tunnel (After Brady and Brown 1993).

tangential displacements, respectively; P_v is the vertical in-situ principal stress; k is the horizontal stress coefficient ($k = P_h/P_v$); E and ν are the Young's modulus and Poisson's ratio, respectively, of the rock mass; r and θ are the polar coordinates of the measurement point; and R is the radius of tunnel cross section; as shown in Fig. 1.

If the in-situ stress is at the hydrostatic pressure condition, or $P_v = P_h = P_o$ (i.e. $k = 1.0$), the tangential displacement, u_θ , disappears and the radial displacement, u_r , is shown as Eq. (3).

$$u_r = -\frac{P_o R^2 (1 + \nu)}{E r} \quad (3)$$

If the measurement point is located on the circumference of the excavation face and the in-situ stress is at hydrostatic pressure condition, Eq. (4) below gives the absolute value of maximum radial displacement, $u_{r\infty}$, behind the excavation face of the tunnel.

$$u_{r\infty} = \frac{P_o R (1 + \nu)}{E} \quad (4)$$

With the same assumptions above, the distribution of radial displacement along the longitudinal axis at any point of the circumference of the tunnel cross section is presented in Fig. 2. It is found in this figure that initial displacement exists approximately 2 times of tunnel diameter in front of the excavation face (unexcavated section); the displacement at the excavation is u_{r0} ; and the displacement reaches its maximum, $u_{r\infty}$, at roughly 2 to 4 times of tunnel diameters behind the excavation face (excavated section).

According to Panet (1993), by dividing the

displacement, u_r , along the longitudinal axis of tunnel with the maximum displacement, $u_{r\infty}$, its relationship with the distance from the excavation face, x , is presented in Eq. (5). This equation is valid only for the section behind excavation face, i.e., the excavated section, and the distance from excavation face in the equation is assumed to be $x \geq 0$.

$$\frac{u_r}{u_{r\infty}} = 0.28 + 0.72 \left[1 - \left(\frac{0.84}{0.84 + x/R} \right)^2 \right] \quad (5)$$

Carranza-Torres and Fairhurst developed the displacement ratio versus. distance from excavation face in the form of Eq. (6) based on the tunnel monitoring data collected and the suggestions of Hoek (2002). This equation is suitable for the estimation of displacements behind the excavation face ($x \leq 0$) and in front of the excavation face ($x \geq 0$).

$$\frac{u_r}{u_{r\infty}} = 0.28 + 0.72 \left[1 - \left(\frac{0.84}{0.84 + x/R} \right)^2 \right] \quad (6)$$

Eq. (5) provides the displacement ratios based on the assumption that the media material is linearly elastic, whereas Eq. (6) is an empirical equation based on in-situ monitoring data. Both equations are correlated to the ratio between the distance from the excavation face and tunnel radius (x/R). The displacement ratio ($u_{r0}/u_{r\infty}$) at the excavation face of tunnel falls between 0.25 and 0.31.

3. Description of case study

Taiwan is located where the Eurasian plate and the Philippine Sea plate meet. There are more mountains and hills on this island than flatlands due to the pushing and shoving between the two tectonic plates. For this, tunnels are an important part of traffic infrastructures. In Taiwan, the expressway system covers more than 1,000 km in length, covering almost all types of geology on this island is presented in Fig. 3; in addition, the tunnels along the expressways come in various shapes of cross section. For this, the expressway tunnels of Taiwan were selected for case study.

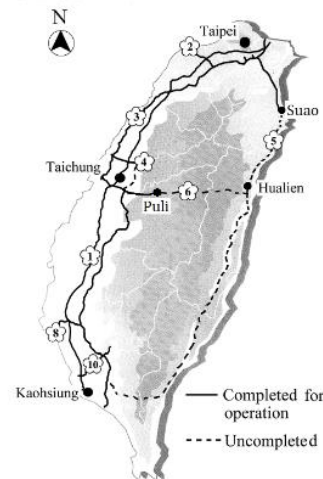


Fig. 3 Taiwan's national expressway network (Freeway Bureau, MOTC)

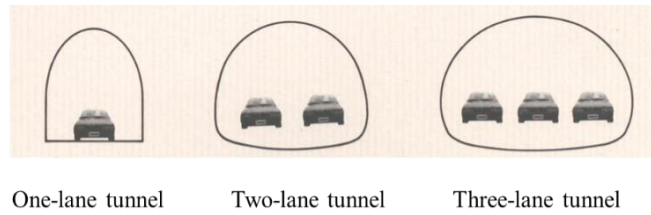


Fig. 4 Schematic drawing showing the different cross-section tunnels

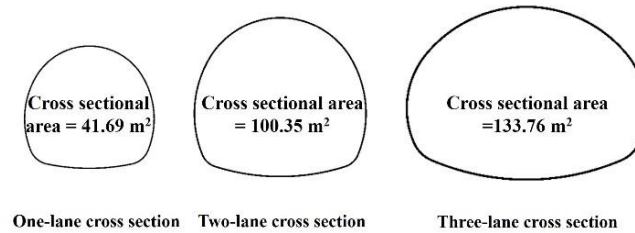


Fig. 5 Cross-sections and excavation areas for the studied tunnels

Table 1 Rock mass classifications

Rock mass class	I	II	III	IV	V	VI
RMR	100-81	80-61	60-41	40-21	20-11	10-0
Geology	Good		Medium		Poor	

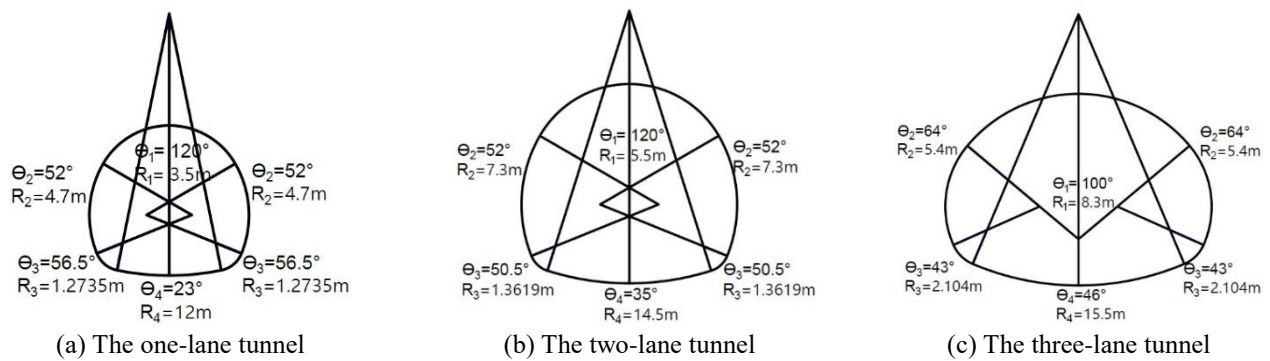


Fig. 6 The geometric data of the cross-section of the tunnel

Table 2 Cross sectional area and round excavation length for the studied tunnels

Cross section	Cross sectional area (m ²)	Equivalent diameter (D _{eq})(m)	Geology	Tunnel name	Round length (m)	Shotcrete thickness (m)
One-lane	41.69	7.29	Good	T1G	2.0	0.12
			Medium	T1M	1.8	0.15
			Poor	T1P	1.5	0.25
Two-lane	100.35	11.30	Good	T2G	1.8	0.15
			Medium	T2M	1.5	0.20
			Poor	T2P	1.2	0.30
Three-lane	133.76	13.05	Good	T3G	1.5	0.20
			Medium	T3M	1.2	0.25
			Poor	T3P	1.0	0.35

3.1 Expressway tunnels of Taiwan

There are more than 40 km of tunnels in length

throughout the expressway network of Taiwan. The expressway network is planned to extend toward the eastern part of Taiwan and mountains in the central part, which

makes tunnels essential to the expansion. The expressway tunnels of Taiwan were mostly excavated by drill and blast method with a cross section similar to a horseshoe shape. Depending on the size of cross section, there are: (1) one-lane cross section, such as pilot tunnels or adits; (2) two-lane cross section; most of the tunnels on the highways in eastern Taiwan or expressways leading to mountains are of two-lane cross section; and (3) three-lane cross section; most of the tunnels on western main lines, such as expressway 3, are of three-lane cross section. The cross sections of the studied tunnels are shown in Figs. 4 and 5. The geometric data of the cross sections are provided in Fig. 6.

The rock mass of the expressway tunnels in Taiwan is classified based on the Rock Mass Rating (RMR). In general, the rock mass surrounding a tunnel is classified in Classes I through VI; the higher the class, the weaker the rock mass. For the convenience of this study, the rock mass is classified into three classes, good, medium and poor, with the RMR ranges shown in Table 1.

As mentioned above, there are one-lane, two-lane and three-lane cross sections for the tunnels and good, medium and poor for rock mass classes. For convenience of this study, T1 stands for one-lane cross section, T2 for two-lane cross section and T3 for three-lane cross section. Added behind T1, T2 and T3, G stands for Good, M for Medium and P for Poor rock mass. For example, the symbol T1G means a one-lane tunnel with good rock mass, whereas T2M represents a two-lane tunnel with medium rock mass; and so on and so forth. There are 9 classes of tunnels investigated in this study with their symbols presented in Table 2.

3.2 Tunnel excavation and support

Tunnels are excavated in rounds as an engineering practice. Considering the stability and workability of a tunnel, the round length depends on the size of cross section and local geology. Generally speaking, a longer round length is possible for small tunnels with good rock mass; or the round length should be shorter for tunnels of large section and poor rock mass. The strutting of mountain tunnels during their excavations are done in two parts, primary support and inner concrete lining. Typically, primary support is considered to balance the pressure from surrounding rock mass in the tunnel analysis and design, unless at the tunnel portal, intersections or where the geology is complicated. Apart from providing extra tunnel stability, the inner concrete lining provides a platform for installation of tunnel lighting, ventilation and traffic control, as well as serves an aesthetic purpose. Table 2 provides the cross-sectional area of excavation, equivalent diameter, D_{equ} , round length and inner lining support (shotcrete) thickness for the 9 types of tunnels investigated in this study. In this study, the equivalent diameter (D_{equ}) is the diameter of the circular cross section converted from the horseshoe-shaped tunnel cross section (A), i.e. $D_{equ} = (4A/\pi)^{1/2}$.

4. Numerical analysis

The numeric analysis was performed using Plaxis 3D

2017, a finite element analysis program developed by Plaxis B.V. The program was first developed by Delf University of Technology in the Netherlands in 1987. It was a 2-dimensional (2D) version at the beginning. After years of evolution, 3D versions of the program have been developed since 2001, including Plaxis 3D Tunnel and Plaxis 3D Foundation. In 2010, the two 3D versions were combined into the Plaxis 3D. This study was carried out with the 2017 version of this program for numeric analysis.

4.1 Numerical analysis assumptions

Tunnel excavation is highly complicated and the variation of surrounding rock mass is significant, not to mention the impact of groundwater. Therefore, theoretical or numerical solution often fails to describe the real situation in the field. The following assumptions were made for the numeric analysis of this study:

- The overburden depth on top of the expressway tunnels in Taiwan varies from several meters up to 750m. This study is aimed to investigate the excavation deformation behaviors of tunnel under different geology. Therefore, the overburden depth is assumed to be 200m for this study:

- It is assumed that the groundwater table is below the invert of tunnel and, therefore, the impact of groundwater is neglected.

- The geotechnical stresses vary from site to site. For this study, the horizontal stress coefficient, k , is assumed to be 1.0 for this study.

- Typically, shotcrete, steel support and rock bolts are used as primary supports in tunnel excavation. For the convenience of study, shotcrete is selected as the primary support and simulated as plate element in the analysis.

- Tunnels are excavated in steps in practice; i.e. in steps of upper half of cross section, bench and invert. For the convenience of study, all tunnels studied are excavated in full cross section.

- It is assumed in the numeric analysis that the excavation has advanced a distance equivalent to one time of the tunnel diameter ($1 D_{equ}$) and the strutting is in place. The subsequent excavation is conducted based on the round lengths provided in Table 2 for individual tunnels, and the total excavation is 3 times of the tunnel diameter ($3 D_{equ}$). For the pre-deformation behaviors of the unexcavated section of tunnel, the scope of numerical analysis extends from the excavation face of the last round to 5 times of tunnel diameter ($5 D_{equ}$) further, thus the total length of tunnel in longitudinal direction $9 D_{equ}$. With T2M (two-lane cross section with medium rock mass) tunnel as an example, the longitudinal profiles is shown in Fig. 7. The Fig. 8 provides the perspective of the constructed section ($1 D_{equ}$) and excavation section ($3 D_{equ}$) of T1G (one-lane cross section with good rock mass) tunnel.

4.2 Material model and parameters

The rock mass is analyzed using the Mohr-Coulomb

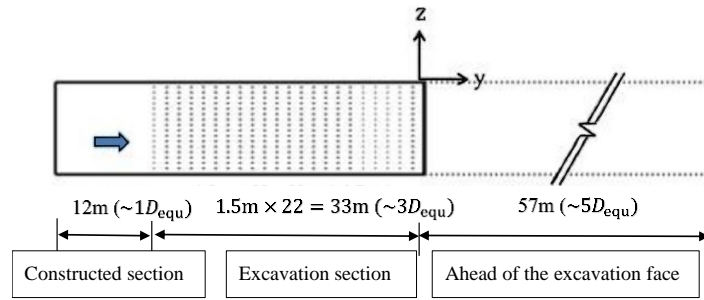


Fig. 7 Schematic representation of the longitudinal sections (Taking T2M as an example)

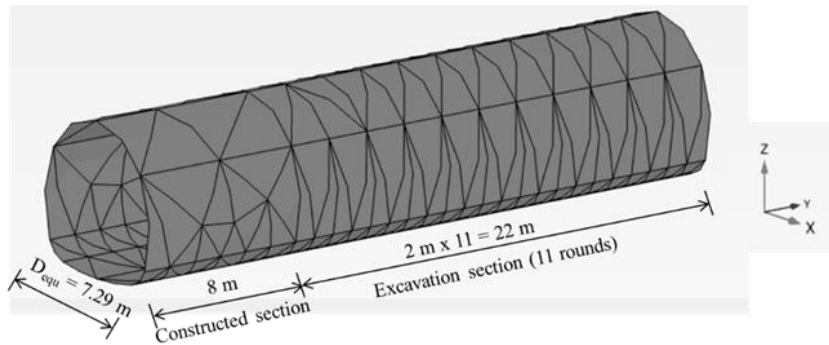


Fig. 8 Perspective view of the constructed and excavation sections of the T1G tunnel

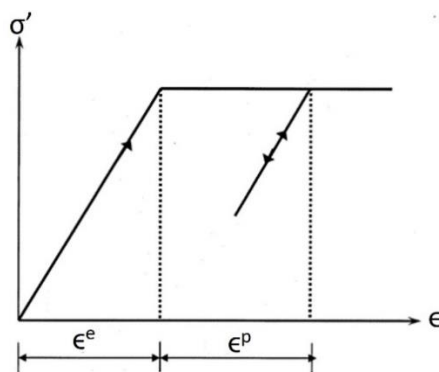


Fig. 9 Basic idea of an elastic perfectly-plastic model

Table 3 Parameters of the Mohr-Coulomb model

Parameter	Unit	Rock mass		
		Good	Medium	Poor
Dry unit weight of rock mass, γ_{dry}	kN/m ³	23	23	23
Wet unit weight of rock mass, γ_{wet}	kN/m ³	25	25	25
Young's modulus of rock mass, E_m	kN/m ²	2.0E6	1.0E6	5.0E5
Poisson's ratio, ν	—	0.25	0.27	0.30
Cohesion, c	kN/m ²	300	150	100
Friction angle, ϕ'	°	33	29	26
Angle of dilatancy, Ψ	°	3	0	0

model and Hoek-Brown model for this study. The parameters needed for the models are described as follows:

4.2.1 Mohr-Coulomb model

The Mohr-Coulomb model is the most used

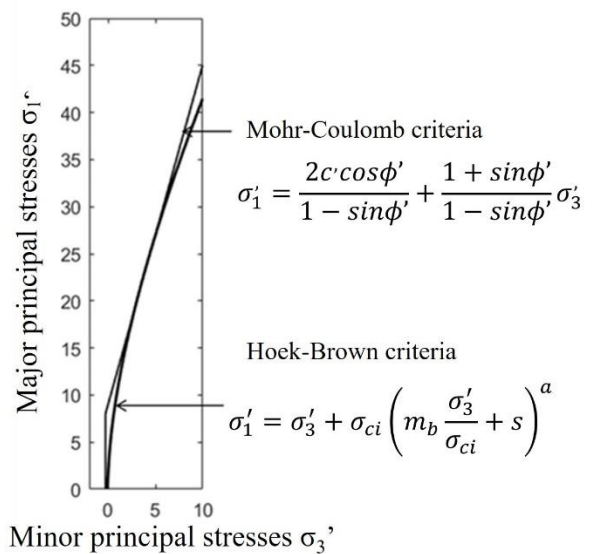


Fig. 10 Relationships between the major and minor principal stresses for the MC and HB criteria (Hoek *et al.* 2002)

fundamental rock mass material model in the numerical analysis of tunnel engineering. The stress vs. strain relationship can be linearly elastic or perfectly plastic, as shown in Fig. 9. The linearly elastic model follows the Hooke's law and the parameters required are the Young's modulus, E , and Poisson's ratio, ν ; whereas the plastic model follows the Mohr-Coulomb criteria of failure. The minimum vs. maximum principal stress of these criteria is described as Eq. (7) and the criteria themselves are the rules of non-associated plasticity. The required strength parameters are cohesion, c , internal friction angle, ϕ' , and

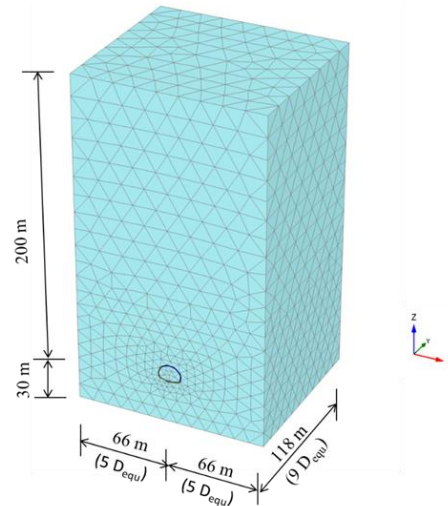


Fig. 11 The generated mesh diagram of the T3P tunnel

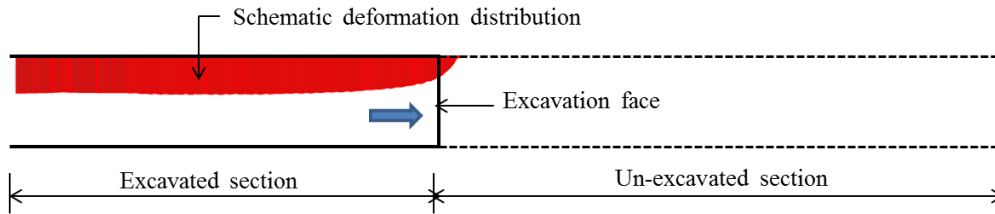


Fig. 12 Schematic drawing showing the longitudinal deformation distribution

Table 4 Parameters of the Hoek-Brown Model

Parameter	Unit	Good rock mass	Medium rock mass	Poor rock mass
Unit weight of rock mass above groundwater table (γ_{unsat})	kN/m ³	23	23	23
Unit weight of rock mass below groundwater table (γ_{sat})	kN/m ³	25	25	25
Young's modulus of rock mass (E_m)	kN/m ²	2.0E6	1.0E6	5.0E5
Poisson's ratio (ν)	—	0.25	0.27	0.30
Uniaxial compressive strength of complete rock (σ_{ci})	kN/m ²	24,000	18,000	12,000
Complete rock parameter (m_i)	—	12	10	8
Geological strength index (GSI)	—	60	45	30
Degree of disturbance (D)	—	0.4	0.3	0.2
Angle of dilatancy at $\sigma_3' = 0$ (Ψ_{max})	°	3	0	0
Confining pressure, σ_3' , at the angle of dilatancy $\Psi = 0^\circ$ (σ_ψ)	kN/m ²	1,150	0	0

Table 5 Shotcrete properties for the studied tunnels

Tunnel name	T1G	T1M	T1P	T2G	T2M	T2P	T3G	T3M	T3P
Shotcrete thickness, t (m)	0.12	0.15	0.25	0.15	0.20	0.30	0.20	0.25	0.35
Unit weight, γ (kN/m ³)	25								
Young's modulus, E (kN/m ²)	2.4E7								
Poisson's ratio, ν	0.17								

angle of dilatancy, ψ . Table 3 provides the parameters needed for the Mohr-Coulomb model for each class of rock mass.

$$\sigma_1' = \frac{2c' \cos \phi'}{1 - \sin \phi'} + \frac{1 + \sin \phi'}{1 - \sin \phi'} \sigma_3' \quad (7)$$

4.2.2 Hoek-Brown model

The Hoek-Brown model was derived from a large quantity of rocks and field experiments. Unlike the Mohr-Coulomb that is more commonly used, the principal stress of Hoek-Brown model is in a nonlinear distribution. Fig. 10 provides a comparison between both models. The failure

criteria of Hoek-Brown model are presented as Eq. (8), where m_b is the reduction of the complete rock parameter, m_i , s and a are associated with Geological strength index (GSI) and Degree of disturbance (D), respectively. If the unit weight of rock mass (γ) and interfacial strength reduction coefficient (R_{inter}) are neglected, the Hoek-Brown model requires 8 parameters, including the Young's modulus of rock mass (E_m), Poisson's ratio (ν), uniaxial compressive strength of rock (σ_{ci}), complete rock coefficient (m_i), geological strength index (GSI), degree of disturbance (D), angle of dilatancy at $\sigma_3' = 0$ (ψ_{max}) and the confining pressure $\sigma_3'(\sigma_\psi)$ at the angle of dilatancy $\psi = 0^\circ$. Table 4 provides the rock mass parameters.

$$\sigma_1' = \sigma_3' + \sigma_{ci} \left(m_b \frac{\sigma_3'}{\sigma_{ci}} + s \right)^a \quad (8)$$

4.2.3 Linearly elastic model

Compared to rock or soil mass, the shotcrete has a greater stiffness and its stress vs. strain follows the elastic model of Hooke's law. Table 5 provides the shotcrete thickness (t), unit weight (γ), Young's modulus (E) and Poisson's ratio (ν) for the 9 types of tunnels studied herein.

4.3 Numerical analysis method and steps

The deformation behaviors of expressway tunnels in Taiwan under different geologies are studied using a 3D FEM analysis program. The following is the description of the method and steps of the numeric analysis:

- Determine the boundaries of analysis section: The horizontal boundary extends 5 times of tunnel diameter ($5 D_{equ}$) on both sides of tunnel centerline along the x -axis. Along the longitudinal axis (y -axis) of the tunnels, it is assumed that the excavation and support have been completed within the distance equivalent to the tunnel diameter. Next, the excavation advances per the round lengths in Table 2 for each tunnel for a total excavation of 3 times of tunnel diameter. For the pre-deformation behaviors of tunnels, the analysis extends 5 more times of tunnel diameter from the excavation face of last round towards the y -direction. Therefore, the boundary length along the longitudinal axis of tunnel is in total 9 times of tunnel diameter ($9 D_{equ}$). In z -direction, it is assumed that the overburden depth above the invert of tunnel is 200m. To avoid boundary disturbance, the boundary along z -direction extends 30m further downwards from the invert. Therefore, the boundary length along the z -direction is 230m in total. With T3P (the three-lane tunnel with poor rock mass) as an example, the boundary length is shown in Fig. 11.

- The rock mass to be analyzed is modeled using Borehole function. Table 3 or 4 provides the parameters that define the rock properties depending on the material model of the rock mass.

- Establish the shape of tunnel cross section and then the tunnel strutting based on the parameters in Table 5.

- Extend the tunnel along the longitudinal axis (y -axis) based on the round lengths in Table 2 and the range to be analyzed.

- Develop the analysis mesh; the mesh herein is developed using medium coarseness, but is refined at the location of excavation. With T3P as an example, the analysis mesh is shown in Fig. 11. The longitudinal deformation distribution is shown in Fig. 12.

- Simulate the tunnel construction in stage; at the end of initial phase, phase 1 represents the section where the construction is completed (length = $1 D_{equ}$). The subsequent rounds of excavation are simulated for each phase. With T2M in Fig. 5 as an example, the excavation is conducted in 22 rounds with the round length of 1.5 m for a total excavation of 33 m (approximately $3 D_{equ}$ long).

- Run analysis; as the analysis comes to an end, select the final phase of excavation and examine its displacement. The result is collected and plots developed based on the target requirements.

5. Numerical analysis results

The magnitude and distribution of stress around the horseshoe-shaped cross section excavated by drill and blast are somewhat different. For the convenience of analysis, only the vertical displacement of tunnel crown, u_z , at Point A is shown in Figs. 13 and 14, is discussed herein. The analysis results of Mohr-Coulomb model and Hoek-Brown model are presented below:

5.1 Mohr-Coulomb model

If the rock mass is analyzed using the Mohr-Coulomb model, the longitudinal distribution of vertical crown displacement (u_z) for the studied cross sections at various geologies are provided in Fig. 15. It is clear in the figure that the greater the tunnel cross section is, the greater the displacement (absolute value); and in the same cross section, the poorer the geology, the greater the displacement.

For a better picture of the magnitude and distribution of displacement along the longitudinal axis (y -axis), Table 6 provides the locations of maximum displacement (u_{z-max}) for each type of tunnel and 10% of maximum displacement ($0.1 * u_{z-max}$) and their locations on the longitudinal axis; this table also provides the displacement at the excavation face (u_{z-f}) for each tunnel and its percentage of the maximum displacement (u_{z-f}/u_{z-max}). It is found in Table 6 that the maximum displacement of each tunnel falls approximately between 3 and 4 times of the tunnel diameter ($3-4 D_{equ}$) behind the excavation face; the ratio between the displacement at the excavation face and the maximum displacement falls between 0.35 and 0.59, and this ratio varies from site to site depending on local geology; the poorer the geology, the greater this ratio. The displacement drops to 10% of the maximum displacement 0.8 to 2.6 times of diameter in front of the excavation face and this distance increase as the geology becomes poorer.

5.2 Hoek-Brown model

If the rock mass is analyzed using the Hoek-Brown

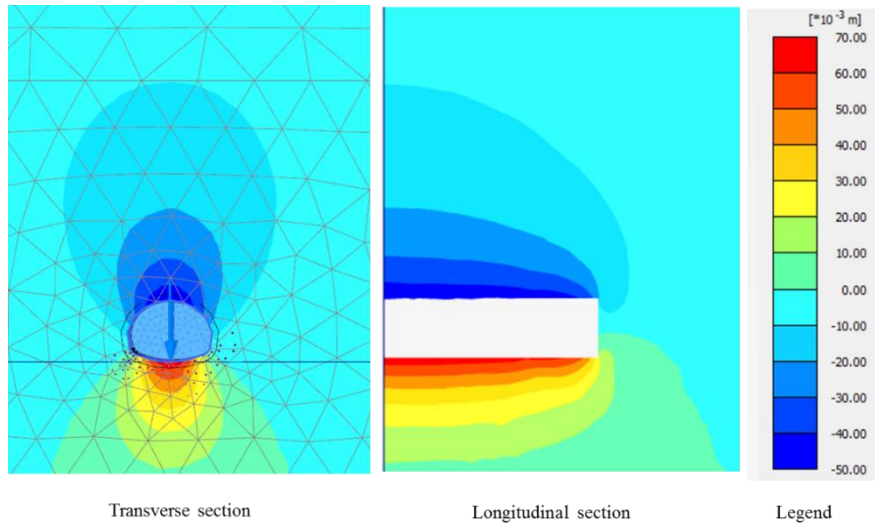


Fig. 13 Shadings of the vertical displacements of the T3P tunnel

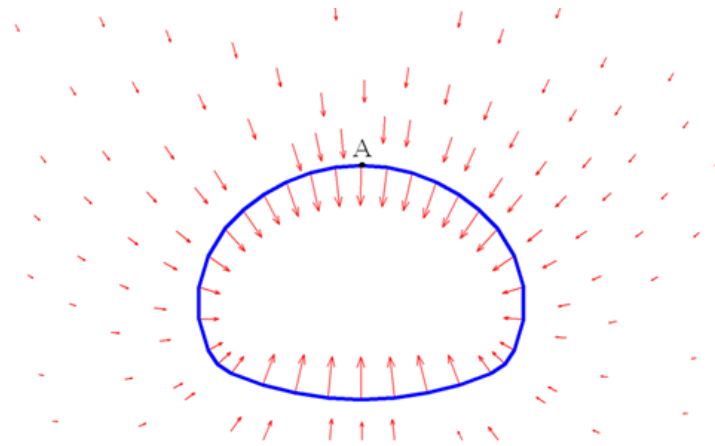


Fig. 14 Schematic drawing showing the cross-sectional deformation distribution

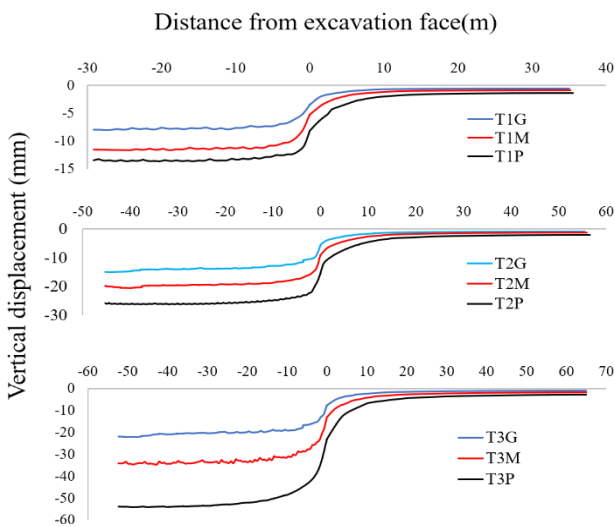


Fig. 15 Deformation distributions of the studied tunnels (Mohr-Coulomb Model)

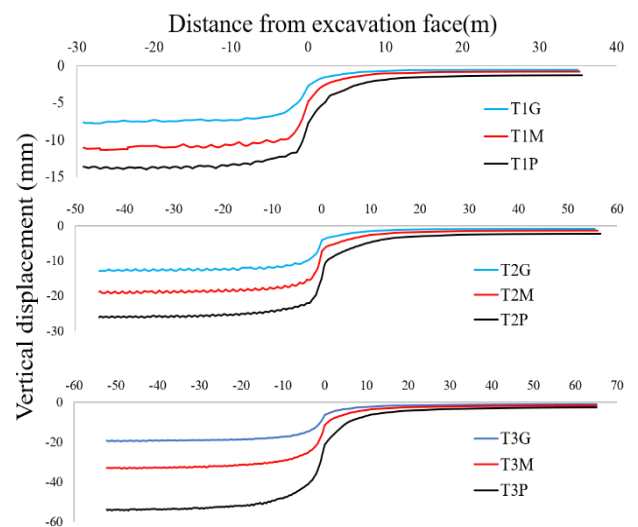


Fig. 16 Deformation distributions of the studied tunnels (Hoek-Brown Model)

model, the longitudinal distribution of vertical crown displacement (u_z) for the studied cross sections at various geologies are provided in Fig. 16. Table 7 provides the

locations of maximum displacement (u_{z-max}) for each type of tunnel and 10% of maximum displacement ($0.1 * u_{z-max}$) and their locations on the longitudinal axis; this table also

Table 6 The displacement characteristics of the studied tunnels (Mohr-Coulomb Model)

Tunnel	D_{equ} (m)	u_{z-max} (mm)	Distance from excavation face for u_{z-max}	u_{z-f} (mm)	u_{z-f}/u_{z-max}	$0.1*u_{z-ax}$ (mm)	Distance from excavation face for $0.1*u_{z-max}$
T1G	7.29	7.98	-27.00 m (-3.70 D_{equ})	3.44	0.43	0.80	7.90 m (1.09 D_{equ})
T1M	7.29	11.64	-24.30 m (-3.33 D_{equ})	5.28	0.45	1.16	10.70 m (1.47 D_{equ})
T1P	7.29	13.66	-20.25 m (-2.78 D_{equ})	8.12	0.59	1.37	18.98 m (2.60 D_{equ})
T2G	11.3	14.95	-44.10 m (-3.90 D_{equ})	5.40	0.36	1.50	11.10 m (0.98 D_{equ})
T2M	11.3	20.69	-39.76 m (-3.52 D_{equ})	9.19	0.44	2.07	15.10 m (1.34 D_{equ})
T2P	11.3	26.25	-31.80 m (-2.81 D_{equ})	15.52	0.59	2.63	24.70 m (2.19 D_{equ})
T3G	13.05	22.00	-47.28 m (-3.62 D_{equ})	7.66	0.35	2.20	10.55 m (0.81 D_{equ})
T3M	13.05	34.74	-42.62 m (-3.27 D_{equ})	13.06	0.38	3.47	12.50 m (0.96 D_{equ})
T3P	13.05	54.05	-39.49 m (-3.03 D_{equ})	23.20	0.43	5.41	14.20 m (1.09 D_{equ})

Table 7 The displacement characteristics of the studied tunnels (Hoek-Brown Model)

Tunnel	D_{equ} (m)	u_{z-max} (mm)	Distance from excavation face for u_{z-max}	u_{z-f} (mm)	u_{z-f}/u_{z-max}	$0.1*u_{z-max}$ (mm)	Distance from excavation face for $0.1*u_{z-max}$
T1G	7.29	7.74	-27.00 m (-3.70 D_{equ})	2.69	0.35	0.77	7.90 m (1.08 D_{equ})
T1M	7.29	11.34	-26.09 m (-3.58 D_{equ})	4.83	0.43	1.13	9.25 m (1.27 D_{equ})
T1P	7.29	13.92	-21.00 m (-2.88 D_{equ})	7.73	0.56	1.39	22.60 m (3.10 D_{equ})
T2G	11.3	12.82	-44.10 m (-3.90 D_{equ})	4.06	0.32	1.28	12.30 m (1.09 D_{equ})
T2M	11.3	19.26	-42.75 m (-3.78 D_{equ})	7.24	0.38	1.93	14.40 m (1.27 D_{equ})
T2P	11.3	26.22	-36.00 m (-3.19 D_{equ})	14.90	0.57	2.62	25.15 m (2.23 D_{equ})
T3G	13.05	19.50	-48.75 m (-3.73 D_{equ})	6.22	0.32	1.95	12.10 m (0.93 D_{equ})
T3M	13.05	33.13	-47.42 m (-3.63 D_{equ})	11.27	0.34	3.31	13.00 m (1.00 D_{equ})
T3P	13.05	54.16	-47.03 m (-3.60 D_{equ})	21.30	0.39	5.42	14.05 m (1.08 D_{equ})

Table 8 The comparison of numerical results between MC and HB models

Tunnel	Model	u_{z-max} (mm)	Distance from excavation face for u_{z-max} (D_{equ})	u_{z-f} (mm)	u_{z-f}/u_{z-max}	$0.1*u_{z-max}$ (mm)	Distance from excavation face for $0.1*u_{z-max}$ (D_{equ})
T1G	MC	7.98	-3.70 D_{equ}	3.44	0.43	0.80	1.09 D_{equ}
	HB	7.74	-3.70 D_{equ}	2.69	0.35	0.77	1.08 D_{equ}
T1M	MC	11.64	-3.33 D_{equ}	5.28	0.45	1.16	1.47 D_{equ}
	HB	11.34	-3.58 D_{equ}	4.83	0.43	1.13	1.27 D_{equ}
T1P	MC	13.66	-2.78 D_{equ}	8.12	0.59	1.37	2.60 D_{equ}
	HB	13.92	-2.88 D_{equ}	7.73	0.56	1.39	3.10 D_{equ}
T2G	MC	14.95	-3.90 D_{equ}	5.40	0.36	1.50	0.98 D_{equ}
	HB	12.82	-3.90 D_{equ}	4.06	0.32	1.28	1.09 D_{equ}
T2M	MC	20.69	-3.52 D_{equ}	9.19	0.44	2.07	1.34 D_{equ}
	HB	19.26	-3.78 D_{equ}	7.24	0.38	1.93	1.27 D_{equ}
T2P	MC	26.25	-2.81 D_{equ}	15.52	0.59	2.63	2.19 D_{equ}
	HB	26.22	-3.19 D_{equ}	14.90	0.57	2.62	2.23 D_{equ}

Table 8 Continued

Tunnel	Model	u_{z-max} (mm)	Distance from excavation face for u_{z-max} (D_{equ})	u_{z-f} (mm)	u_{z-f}/u_{z-max}	$0.1*u_{z-max}$ (mm)	Distance from excavation face for $0.1*u_{z-max}$ (D_{equ})
T3G	MC	22.00	-3.62 D_{equ}	7.66	0.35	2.20	0.81 D_{equ}
	HB	19.50	-3.73 D_{equ}	6.22	0.32	1.95	0.93 D_{equ}
T3M	MC	34.74	-3.27 D_{equ}	13.06	0.38	3.47	0.96 D_{equ}
	HB	33.13	-3.63 D_{equ}	11.27	0.34	3.31	1.00 D_{equ}
T3P	MC	54.05	-3.03 D_{equ}	23.20	0.43	5.41	1.09 D_{equ}
	HB	54.16	-3.60 D_{equ}	21.30	0.39	5.42	1.08 D_{equ}

Table 9 The ratios of u_z to u_{z-max} along the longitudinal axis of the studied tunnels (Averages of MC and HB models)

Tunnel	Distance from excavation face (in D_{equ})														
	-4.0	-3.0	-2.0	-1.5	-1.0	-0.5	-0.25	0	0.25	0.5	1.0	2.0	3.0	4.0	5.0
T1G	1.00	0.97	0.95	0.95	0.92	0.84	0.72	0.39	0.23	0.17	0.11	0.08	0.07	0.07	0.07
T1M	1.00	0.97	0.96	0.95	0.94	0.86	0.81	0.44	0.27	0.19	0.12	0.09	0.08	0.08	0.08
T1P	1.00	1.00	0.99	0.97	0.95	0.90	0.86	0.58	0.39	0.28	0.18	0.11	0.10	0.10	0.09
T2G	1.00	0.96	0.95	0.94	0.91	0.83	0.74	0.34	0.23	0.16	0.10	0.07	0.06	0.06	0.06
T2M	1.00	0.96	0.95	0.95	0.93	0.87	0.79	0.41	0.27	0.19	0.12	0.08	0.07	0.07	0.06
T2P	1.00	0.99	0.99	0.97	0.95	0.92	0.83	0.58	0.33	0.26	0.16	0.11	0.09	0.08	0.08
T3G	1.00	0.97	0.94	0.92	0.89	0.83	0.71	0.34	0.20	0.15	0.09	0.06	0.05	0.05	0.05
T3M	1.00	0.99	0.96	0.95	0.90	0.83	0.73	0.36	0.22	0.15	0.09	0.06	0.05	0.05	0.05
T3P	1.00	1.00	0.98	0.96	0.93	0.83	0.74	0.41	0.25	0.18	0.11	0.07	0.06	0.05	0.05

Table 10 The ratios of u_z to u_{z-max} along the longitudinal axis for different geology (Averages of MC and HB models)

Rock condition	Distance from excavation face (in D_{equ})														
	-4.0	-3.0	-2.0	-1.5	-1.0	-0.5	-0.25	0	0.25	0.5	1.0	2.0	3.0	4.0	5.0
Good	1.00	0.97	0.95	0.94	0.91	0.83	0.72	0.36	0.22	0.16	0.10	0.07	0.06	0.06	0.06
Medium	1.00	0.97	0.96	0.95	0.92	0.85	0.78	0.40	0.25	0.18	0.11	0.08	0.07	0.07	0.06
Poor	1.00	1.00	0.99	0.97	0.94	0.88	0.81	0.52	0.32	0.24	0.15	0.10	0.08	0.08	0.07

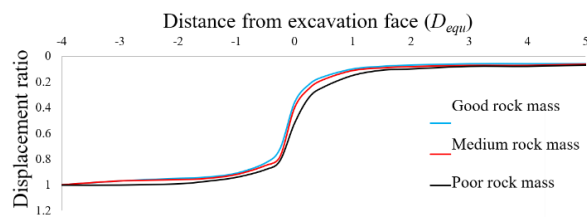


Fig. 17 Average ratios of u_z/u_{z-max} for different geological conditions

provides the displacement at the excavation face (u_{z-f}) for each tunnel and its percentage of the maximum displacement (u_{z-f}/u_{z-max}). It is clear in the figure that the maximum displacement occurs approximately at 3 to 4 times of tunnel diameter behind the excavation face for each of these tunnels; the ratio between displacement at excavation face and maximum displacement falls between 0.32 and 0.57. The displacement drops to 10% of maximum displacement at roughly 0.9 to 3.1 times of tunnel diameters in front of the excavation face, and the longitudinal displacement profile (*LDP*) is in general the same as that of the MC model.

5.3 Comparison between Mohr-Coulomb and Hoek-Brown in terms of analysis result

The results of tunnel analysis using the Mohr-Coulomb (MC) model and Hoek-Brown (HB) model are shown in Table 8. While the failure parameters entered for each of these models are different, the difference in the analysis results is not significant. Particularly, the results are very similar after normalization. The following section will discuss the data analysis after normalization.

5.4 Tunnel displacement analysis after normalization

The longitudinal displacement profiles are normalized in Figs. 15 and 16, i.e., dividing the horizontal distance of the lateral coordinate with the equivalent diameter of cross section and displacement of longitudinal coordinate with the maximum displacement of tunnel. The horizontal coordinate is in D_{equ} and vertical coordinate in u_z/u_{z-max} . The data of both MC and HB models after normalization are averaged and presented in Table 9. It is shown in this table that the displacement ratio (u_{z-f}/u_{z-max}) at the excavation face

is located between 0.34 and 0.58; the poorer the geology, the higher the ratio. Within half of tunnel diameter behind the excavation face (i.e. the excavated section) ($-0.5 D_{equ}$), the u_z/u_{z-max} increases dramatically, while this ratio approaches 1.0 beyond 3 times of tunnel diameter behind the excavation face ($-3 D_{equ}$).

The u_z/u_{z-max} is larger than 0.2 at a quarter of tunnel diameter ($0.25 D_{equ}$) in front of the excavation face; the displacement ratio is still greater than 0.15 at half of tunnel diameter in front of the excavation face; but the ratio gradually decreases to 0.1 one tunnel diameter in front of excavation face. This ratio falls between 0.05 and 0.09 beyond 3 times of tunnel diameter in front of excavation face. For the excavation of a rock tunnel, such a displacement has negligible impact on the stability of typical structures at close proximity.

The displacement ratio (u_z/u_{z-max}) varies not only with the distance from the excavation face, but also with the geology. The ratios of three tunnel cross sections under the same geology in Table 9 are averaged and presented in Table 10. It is shown in this table that the displacement ratio (u_z/u_{z-max}) at the excavation face are 0.36, 0.40 and 0.52 for good, medium and poor rock masses, respectively. The difference in the displacement ratios due to geological variation is significant between 0.5 time of tunnel diameter behind ($-0.5 D_{equ}$) and in front of ($0.5 D_{equ}$) the excavation face. The LDPs of different rock masses after normalization are shown in Fig. 17.

6. Conclusions

This study is intended to investigate the deformation behaviors of tunnel excavation using 3D FEM program. The subject of study is the mountain tunnels throughout the expressway systems of Taiwan. The tunnels studied have one-lane, two-lane and three-lane cross sections and each of these cross sections are classified as good, medium and poor in terms of geology. The numeric analysis is performed with two material models, Mohr-Coulomb and Hoek-Brown. The analysis is concluded as followed:

- If analysis assumptions are reasonable and appropriate material parameters are selected, the result of numeric analysis on mountain tunnels displays no significant difference between the Mohr-Coulomb and Hoek-Brown models, and the distributions of LDP are relatively the same.
- The tunnel cross section and geology play an important part in the tunnel excavation deformation behaviors. Generally speaking, tunnels with a large cross section and located in poor rock mass tend to have large displacement due to excavation; on the other hand, those with a small cross section and located in good rock mass tend to have smaller displacement.
- The initial deformation of tunnel has occurred several times of tunnel diameter in front of the excavation face. Approximately 3 times of tunnel diameter in front of excavation face, the displacement ratio (displacement at this point divided by the maximum displacement of the tunnel)

exceeds 0.05; this ratio is more than 0.1 one tunnel diameter in front of the excavation face.

- The displacement ratio at the excavation face of tunnel falls between 1/3 and 1/2. This ratio depends on local geology. The displacement ratios at the excavation face are 0.36, 0.40 and 0.52 for good, medium and poor rock masses, respectively.
- If time-dependent factors are neglected, the displacement ratio at half of tunnel diameter behind the excavation face increases steeply; the displacement reaches its maximum 3 to 4 times of tunnel diameter behind the excavation face; i.e., the displacement ratio mentioned above approaches 1.0.
- Geology is indeed one of the most important factors in tunnel excavation behaviors. Not only the constructor shall have basic understanding of geology, but also the geological survey during the engineering design phase shall be thorough and carefully planned. In addition, attention is required for the rock mass classification and measurement during the construction phase.

References

- Basarir, H., Genis, M. and Ozarlan, A. (2010), "The analysis of radial displacements occurring near the face of a circular opening in weak rock mass", *Int. J. Rock Mech. Min. Sci.*, **47**(5), 771-783. <https://doi.org/10.1016/j.ijrmmms.2010.03.010>.
- Bieniawski, Z.T. (1989). *Engineering Rock Mass Classification*, John Wiley & Sons, New York, U.S.A., 51-68.
- Brady, B.H.G. and Brown, E.T. (1993), *Rock Mechanics for Underground Mining (2nd ed)*, Chapman and Hall, London, U.K.
- Brinkgreve, R.B.J. (2017), *Plaxis Manual-General Information*, Plaxis B.V., Delft, The Netherlands.
- Brinkgreve, R.B.J. (2017), *Plaxis Material Models Manual*, Plaxis B.V., Delft, The Netherlands.
- Carranza-Torres, C. and Fairhurst, C. (2000), "Application of the convergence-confinement method of tunnel design to rock masses that satisfy the Hoek-Brown failure criterion", *Tunn. Undergr. Sp. Technol.*, **15**(2), 187-213. [https://doi.org/10.1016/S0886-7798\(00\)00046-8](https://doi.org/10.1016/S0886-7798(00)00046-8).
- Chen, S.L., Lee, S.C. and Gui, M.W. (2009), "Effect of rock pillar width on the excavation behavior of parallel tunnels", *Tunn. Undergr. Sp. Technol.*, **24**(2), 148-154. <https://doi.org/10.1016/j.tust.2008.05.006>.
- Ding, L. and Liu, Y. (2018), "Study on deformation law of surrounding rock of super long and deep buried sandstone tunnel", *Geomech. Eng.*, **16**(1), 97-104. <https://doi.org/10.12989/gae.2018.16.1.097>.
- Eberhardt, E. (2012), "The Hoek-Brown failure criterion", *Rock Mech. Rock Eng.*, **45**(6), 981-988. <https://doi.org/10.1007/s00603-012-0276-4>.
- Hoek E., Carranza C. and Corkum B. (2002), "Hoek-Brown failure criterion-2002 edition", *Proceedings of the NARMS-TAC Conference*, Toronto, Ontario, Canada, July.
- Hoek, E. (2007), *Practical Rock Engineering, Chapter of Rock Mass Properties*, Evert Hoek Consulting Engineer Inc., North Vancouver, British Columbia, Canada.
- Lee, S.C. and Tseng, D.J. (2011), "Review and perspective of expressway in Taiwan", *J. Rock Mech. Geotech. Eng.*, **3**(1), 385-397. <https://doi.org/10.3724/SP.J.1235.2011.00385>.
- Panet, M. (1993), *Understanding Deformations in Tunnels*, in

- Comprehensive Rock Engineering*, (Vol. 1), Pergamon, London, U.K., 663-690.
- Sadeghiyan, R., Hashemi, M. and Moloudi, E. (2016), "Determination of longitudinal convergence profile considering effect of soil strength parameters", *Int. J. Rock Mech. Min. Sci.*, **82**, 10-21. <https://doi.org/10.1016/j.ijrmms.2015.10.011>.
- Taiwan Area National Expressway Engineering Bureau, MOTC (2004), *Second Highway Construction Album-Tunnel and Geoengineering*, Taipei, Taiwan (ROC), 68-72.
- Taiwan Area National Expressway Engineering Bureau, MOTC (2006), *Beiyi Expressway Construction (Technical Edition), Tunnel Engineering*, Taipei, Taiwan (ROC), 59.
- Taiwan Area National Expressway Engineering Bureau, MOTC (2013), *Technical Practice of National Highway Geoengineering*, Taipei, Taiwan (ROC), 87-140.
- Unlu, T. and Gercek, H. (2003), "Effect of Poisson's ratio on the normalized radial displacements occurring around the face of a circular tunnel", *Tunn. Undergr. Sp. Technol.*, **18**(5), 547-553. [https://doi.org/10.1016/S0886-7798\(03\)00086-5](https://doi.org/10.1016/S0886-7798(03)00086-5).
- Yoo, C. and Choi, J. (2018), "Effect of construction sequence on three-arch tunnel behavior – Numerical investigation", *Geomech. Eng.*, **15**(3), 911-917. <https://doi.org/10.12989/gae.2018.15.3.911>.